diameters with the mass spectra. Another important question raised by these results is that of the degree of sphericity of the various giant fullerenes, which requires further investigation.

REFERENCES AND NOTES

1. D. H. Parker *et al.*, *J. Am. Chem. Soc.* **113**, 7499 (1991).
2. C. Smart *et al.*, *Chem. Phys. Lett.*, in press.
3. S. Wang and P. R. Buseck, *ibid.* **182**, 1 (1991).
4. S. Iijima, *Nature* **354**, 56 (1991).
5. J. W. Mintmire, B. I. Dunlap, C. T. White, *Phys. Rev. Lett.* **68**, 631 (1991).
6. J. L. Wragg, J. E. Chamberlain, H. W. White, W. Krätschmer, D. R. Huffman, *Nature* **348**, 623 (1990).
7. R. S. Ruoff, T. Randolph, W. R. Creasy, unpublished results.
8. W. Krätschmer, L. D. Lamb, K. Fostiropoulos, D. R. Huffman, *Nature* **347**, 354 (1990).
9. R. Disch and J. M. Schulman, *Chem. Phys. Lett.* **125**, 465 (1986).
10. T. Chen *et al.*, *J. Vac. Sci. Technol. B* **9**, 2461 (1991).

11. We thank R. S. Ruoff for suggesting the use of high-pressure vessels for high-temperature extractions, C. Becker for providing the mass spectral data, and D. Lichtenberger and Q. Fernando for valuable discussions. One of us (D.S.) also thanks the Air Force Office of Scientific Research, the Office of Naval Research, and the Joint Services Optical Program for partial support of this work. The STMs used in these experiments were supplied by Digital Instruments Inc. and McAllister Technical Services.

24 January 1992; accepted 21 February 1992

Surface Charge–Induced Ordering of the Au(111) Surface

JIA WANG, ALISON J. DAVENPORT, HUGH S. ISAACS, B. M. OCKO*

Synchrotron surface x-ray scattering (SXS) studies have been carried out at the Au(111)/electrolyte interface to determine the influence of surface charge on the microscopic arrangement of gold surface atoms. At the electrochemical interface, the surface charge density can be continuously varied by controlling the applied potential. The top layer of gold atoms undergoes a reversible phase transition between the (1 × 1) bulk termination and a (23 × $\sqrt{3}$) reconstructed phase on changing the electrode potential. In order to differentiate the respective roles of surface charge and adsorbates, studies were carried out in 0.1 M NaF, NaCl, and NaBr solutions. The phase transition occurs at an induced surface charge density of 0.07 ± 0.02 electron per atom in all three solutions.

THE UTILIZATION OF SXS, SCANNING tunneling microscopy (STM), and atomic force microscopy techniques during the past decade has greatly enhanced our understanding of surfaces in vacuum. These same techniques are also being used to study electrode surfaces on an atomic scale with an increasing level of sophistication (*1–5*). We report the principal results of a comprehensive SXS study of the Au(111) electrode surface in aqueous electrolytes. In an SXS measurement the diffracted intensity distribution couples directly to the periodicity of the top several layers of metal atoms so that the phase behavior versus the applied potential can be measured directly with a high degree of accuracy. The phase behavior of the Au(111) electrode versus the induced surface charge exhibits universal behavior, independent of the solution species. These findings may have general applicability to vacuum and electrochemical surfaces.

The vacuum atomic arrangement of Au atoms at the Au(111) surface has been obtained from STM measurements (*6, 7*) and from a variety of diffraction techniques including low-energy electron diffraction (LEED) (*8, 9*), transmission electron diffraction (*10*), He scattering (*11*), and SXS (*12, 13*). The observed diffraction peaks have been interpreted as indicating a rectangular (23 × $\sqrt{3}$) unit cell corresponding to a uniaxial compression (4.4%) along the <1,0,0> direction (hexagonal coordinates) (Fig. 1A). Recent SXS (*12*) and STM studies (*6*), in vacuum, have revealed that the direction of the uniaxial compression rotates by ±60° to form a regular array of kink dislocations.

The possibility that Au surfaces might reconstruct under electrochemical conditions was postulated on the basis of the hysteresis in capacity-potential curves (*14, 15*). Ex situ LEED studies have shown that the Au(111) surface, after emersion from an electrochemical cell, forms a (23 × $\sqrt{3}$) phase in the negative potential regime (*16*). Recently, second-harmonic generation (SHG) measurements (*17, 18*) have demonstrated that the phase transition between the (23 × $\sqrt{3}$) phase and the (1 × 1) phase can be monitored in situ by the additional symmetry pattern in the SHG intensity associated with the uniaxial compressed phase. However, it is difficult to extract detailed structural information from ex situ and SHG studies. Concurrent with the present SXS study, in situ STM studies (*19, 20*) in $HClO_4$ solutions have confirmed the existence of the (p × $\sqrt{3}$) reconstruction within the negative potential regime. The precision in this SXS study of the Au(111) electrode is beyond the capabilities of any of the previous probes. The experimental approach is described in (*4, 21, 22*). The applied potential is referenced to an Ag/AgCl(3 M KCl) electrode.

In a surface diffraction measurement, the (p × $\sqrt{3}$) reconstruction gives rise to additional in-plane reflections beyond the underlying (1 × 1) reflections. As demonstrated (*9*), the reconstruction reflections are arranged in a hexagonal pattern surrounding the integer (H, K) positions (Fig. 1B). In Fig. 1C, equal intensity contour lines are shown in the vicinity of the (0,1) reflection for a 0.01 M NaCl solution at −0.3 V. Four reflections surrounding the (0,1) reflection are arranged in a hexagonal pattern, where δ is the length of a hexagonal side (dimensionless units). This pattern is consistent with a (23 × $\sqrt{3}$) unit cell without the additional features expected for a regular array of discommensuration kinks (*12*). At the most positive applied potentials, the reconstruction peaks coalesce at the integer positions.

We investigated the potential dependence of the diffraction pattern by measuring the scattering profile through the (0,1) reflection along the <1,1> direction (Fig. 1C). Along this axis (defined as q_r) the scattering wave vector is given by ($q_r/\sqrt{3}$, 1 + $q_r/\sqrt{3}$). In Fig. 2A, the measured scattering intensity is shown at a series of decreasing potentials between 0.1 and −0.8 V in a 0.01 M NaCl solution. At potentials of 0.10 V and above, the scattering is centered at q_r = 0, which indicates that the surface is not reconstructed. As the potential is reduced below 0.05 V, a second peak emerges, corresponding to the reconstructed phase (see Fig. 1C). Concomitantly, the (0,1) reflection decreases in intensity. The peak position of the reconstruction, ($\delta/\sqrt{3}$, 1 + $\delta/\sqrt{3}$), moves outward (increased compression), and the peak sharpens (increased order) as the potential is decreased.

In order to extract the stripe separation p, the scattering profiles have been described as the sum of two Lorentzians (*21*) (centered at zero and δ). Fits to the Lorentzian form (solid lines in Fig. 2A) describe most of the

J. Wang and B. M. Ocko, Department of Physics, Brookhaven National Laboratory, Upton, NY 11973.
A. J. Davenport and H. S. Isaacs, Department of Applied Science, Brookhaven National Laboratory, Upton, NY 11973.

*To whom correspondence should be addressed.

essential features of the profiles. The dependence of the fitted stripe separation, $p = \sqrt{3}/(2\delta)$, is shown in Fig. 2B. Although the transition is reversible, the measured p depends on the sweep direction as indicated in the figure. After the initial signs of the surface reconstruction at 0.05 V, which correspond to the emergence of the modulation peak, there is a continued compression as the potential is decreased, as shown by the inverted triangles in Fig. 2B. The maximum observed compression corresponds to $p = 23$ ($\delta = 0.038$). This result is identical to that of the vacuum studies. This observation suggests that under both electrochemical and vacuum conditions the Au(111) surface has the same underlying surface motif. As the potential is increased above −0.1 V, p increases and reaches a value of 25 at 0.15 V. Above 0.20 V the striped phase is no longer stable.

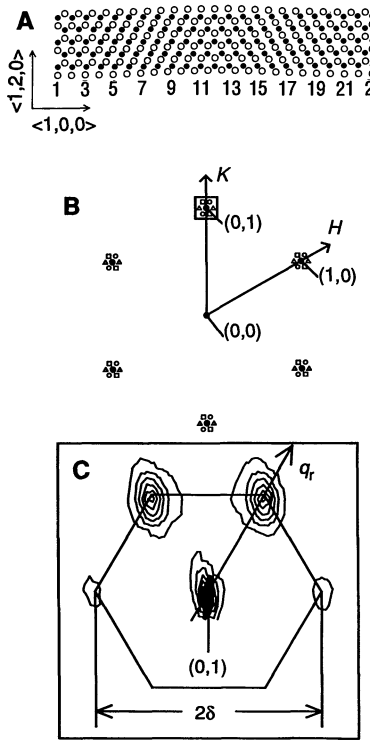

Fig. 1. (**A**) In-plane hexagonal structure of the Au(111) surface. The solid (open) circles correspond to atoms in the second (first) layer. Surface atoms in the left and right sides of the figure are in undistorted hexagonal sites (ABC stacking sequence), whereas in the center of the figure the atoms are in faulted sites (ABA stacking sequence) (*11, 12*). For 24 surface atoms in place of 23 underlying surface atoms along the <11> direction, the compression is 24/23 − 1 = 4.4% and $\delta = (\sqrt{3}/2)/23 = 0.038$. (**B**) In-plane diffraction pattern from the Au(111) surface. Solid circles represent diffraction from the underlying hexagonal lattice. Open symbols originate from the (23 × $\sqrt{3}$) reconstructed phase with three rotational equivalent domains (circles, squares, and triangles). The axis, q_r, is defined to be along the <1,1> direction. (**C**) Equal-intensity scattering contours in the vicinity of the (0,1) reflection at $L = 0.5$ measured in 0.01 M NaCl at −0.3 V versus a saturated Ag/AgCl reference electrode.

We observe a significant increase in the correlation length—decrease in the width of the peak at δ—and a small decrease in p by cycling the potential within the reconstructed potential regime. We refer to the surface state where the maximum compression and correlation length are achieved as the groomed surface. Specular reflectivity measurements (*22*) in these same solutions at the Au(111) surface show that this process involves only a rearrangement of the Au atoms within the surface plane. In $HClO_4$, LiCl, CsCl, NaF, NaCl, and NaBr solutions, the minimum stripe length, observed after preparing a groomed surface, is $p = 23$. Therefore, cation and anion species do not affect the structure of the reconstructed Au(111) surface. However, the phase transition potential depends on the anion species and not the cation species (*22*). Cation species remain nearly fully hydrated at the interface and do not specifically adsorb. This is confirmed by capacitance data with K^+ and Na^+ salts which are invariant to the cation species (*23*).

Figure 3B shows the potential dependence of the scattered intensity at ($0.038/\sqrt{3}$, $1 + 0.038\sqrt{3}$, 0.2) in 0.1 M NaF, NaCl, and NaBr solutions. The transition potential decreases in the order $F^- > Cl^- > Br^-$. In addition, the hysteresis between the negative and positive sweep directions decreases in the same order. An initial increase in the scattered intensity (negative sweep) corresponds to the formation of a reconstructed phase with $p \approx 27$. This feature appears at a potential of 0.18 ± 0.05 V (NaF), 0.02 ± 0.04 V (NaCl), and −0.18 ± 0.03 V (NaBr). As p decreases to 23, there is a further increase in the scattered intensity. In the positive sweep direction, the intensity at ($0.038/\sqrt{3}$, $1 + 0.038\sqrt{3}$, 0.2) starts to decrease when p starts to expand. The (1 × 1) phase does not completely recover until 0.45 V (NaF), 0.25 V (NaCl), and 0.00 V (NaBr).

Previous interfacial capacitance studies at the Au(111) surface in salt solutions (*24, 25*) are reproduced in Fig. 3A. The potential at the capacitance minimum, in a nonadsorbing electrolyte, is generally accepted as the potential of zero charge (PZC), where there is no excess charge at the metal surface. Fluoride ions do not significantly adsorb at an Au electrode because there is only a slight shift in the capacitance minimum (at about 0.37 V) as the concentration increases from 0.002 to 0.05 M (*25*). In 0.1 M solutions, Cl^- and Br^- start to adsorb at −0.1 and −0.25 V, respectively, as indicated by the large change in slope of the capacitance curve (see Fig. 3A). The scattered x-ray intensity in NaBr (Fig. 3B) does not start to fall until −0.17 V, which indicates that the reconstruction is stable after the onset of anion adsorption. In contrast, the reconstruction starts to lift at 0.1 V in 0.1 M NaF where there is no F^- adsorption because this potential is sufficiently negative of the PZC (0.37 V). These findings suggest that the reconstruction and lifting transition cannot be understood in terms of anion adsorption alone.

The reconstruction and lifting transition can be directly related to the induced surface charge, $\sigma(E)$, independent of the anion species. The induced surface charge density has been obtained by integrating the capacitance curve from the potential of zero charge (PZC) to E, that is,

$$\sigma(E) = \int_{PZC}^{E} C(E')dE'$$

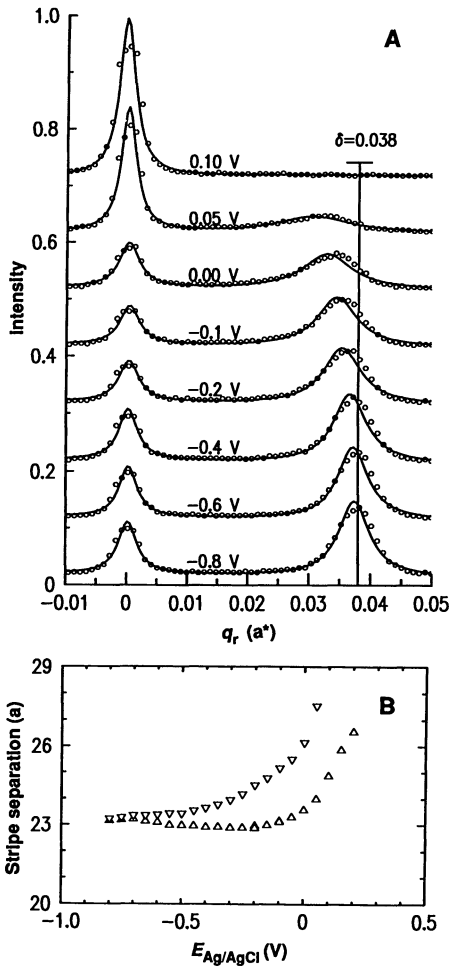

Fig. 2. (**A**) Representative x-ray scattering profiles along the q_r axis (see Fig. 1C) at $L = 0.2$ in 0.01 M NaCl solution at a series of potentials chosen from scans between 0.1 and −0.8 V. The solid lines are fits to a Lorentzian line shape. The effective scan rate is 0.5 mV/s. (**B**) The stripe separation obtained from fitting the data to a sum of two Lorentzians. The triangles and upside-down triangles correspond to positive and negative potential sweeps, respectively.

where E is a potential, E' is a dummy variable for integration, and C is capacitance. This relation is correct in weakly adsorbing electrolytes and nonadsorbing electrolytes, such as 0.1 M NaF (*22*). For the Cl^- and Br^- electrolytes we assume that the surface charge at −0.8 V is the same as in the 0.1 M NaF solution and integrate from this point.

The relation between surface charge and the surface reconstruction is apparent from Fig. 4 where the intensity at $(0.038/\sqrt{3}, 1 + 0.038\sqrt{3}, 0.2)$, acquired as a function of potential, is displayed versus the integrated surface charge. At a surface charge density of ≈0.07 e/atom (excess electrons), in all solutions, the reconstructed $(p \times \sqrt{3})$ phase starts to form. This is indicated by the initial rise in the scattered intensity in Fig. 4. The discrepancy in the scattered intensity above 0.07 e/atom for the different electrolytes is due to differences in p and the degree of surface order. In part, these differences are related to kinetic effects (*22*). In NaF and NaCl electrolytes the reconstruction starts to lift (an increased stripe spacing) at σ = +0.07 e/atom. This transition occurs at σ = +0.05 e/atom in NaBr solutions. In all electrolytes the reconstruction is almost completely lifted by zero surface charge. The appearance of the reconstructed surface at a common value of σ in all three 0.1 M electrolytes suggests a simple phase transition mechanism based on the excess surface charge.

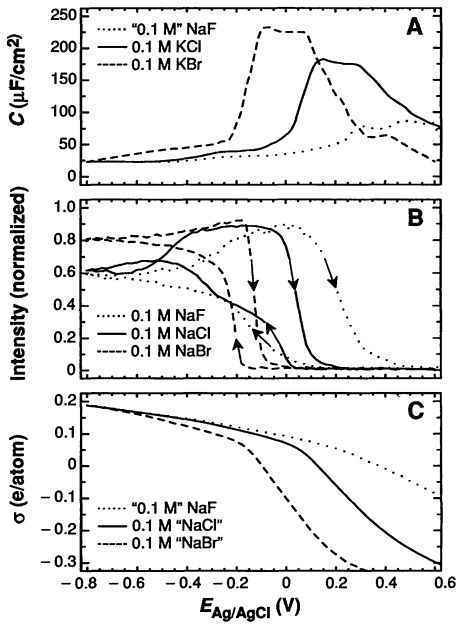

Fig. 3. (**A**) Capacitance of the Au(111) electrode versus the applied potential. The "0.1 M" NaF curve is the mean average of 0.05 M NaF capacitance data from (*25*) and 0.5 M capacitance data from (*24*). The KCl and KBr capacitance data are from (*24*). (**B**) Reconstructed scattering intensity at $(0.038/\sqrt{3}, 1 + 0.038\sqrt{3}, 0.2)$, normalized to the groomed state versus applied potential in three 0.1 M electrolyte solutions. (**C**) Surface charge, $\sigma(E)$, of the Au(111) electrode versus the applied potential in 0.1 M electrolyte solutions calculated from the capacitance. The "NaCl" and "NaBr" surface charges have been calculated from the KCl and KBr data shown in (A). This procedure is valid because these cation species do not significantly affect the capacitance curves.

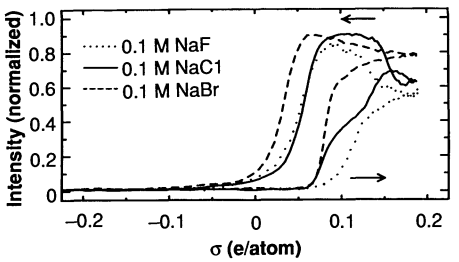

Fig. 4. Scattering intensity at $(0.038/\sqrt{3}, 1 + 0.038\sqrt{3}, 0.2)$ versus the induced surface charge derived from data presented in Fig. 3.

The idea that excess surface charge might induce surface atoms to form a structure different from that of the underlying bulk layers, that is, a reconstructed surface, has been discussed in calculations by Fu and Ho using a local-density-functional (LDF) model (*26*). For Ag(110) they predict that the missing-row structure, absent at the clean metal surface, is induced by alkali adsorbates with an induced surface charge of ≈0.05 e/atom. Within the context of the LDF model, adsorbates in vacuum mimic an applied electric field. At a metal-electrolyte interface, electric fields as high as 10^7 V/cm are accessible and the induced surface charge can exceed 0.2 e/atom.

In vacuum where there is no excess surface charge, all three low-index faces of Au form reconstructed surfaces with a higher packing density than the corresponding (1 × 1) surface (*13, 27*). It is believed that the accumulation of delocalized *sp* electrons in the valleys between surface atoms (*28*) increases the in-plane *sp* bonding, which favors the more densely packed reconstructed state. Therefore, at a negatively charged Au electrode (positive σ) the reconstruction is favored because the excess electrons are accumulated in the valleys (*29*). A positive surface charge leads to a weakened in-plane *sp* bonding, hence the reconstruction is lifted. As such, anion adsorption is indirectly responsible for the lifting through the induced positive surface charge.

The results of our investigation of the phase behavior of the Au(111) electrode surface in 0.1 M NaF, NaCl, and NaBr solutions with in situ x-ray scattering techniques support a phase transition between a reconstructed and ideally terminated surface at a charge density of 0.07 ± 0.02 e/atom. It remains a mystery why the vacuum Au(111) surface (uncharged) exhibits a $(23 \times \sqrt{3})$ pattern, whereas at the solution interface a (1 × 1) state is observed at the PZC.

REFERENCES AND NOTES

1. M. F. Toney *et al.*, *Langmuir* **7**, 796 (1991), and references therein.
2. J. Wiechers, T. Twomey, D. M. Kolb, B. J. Behm, *J. Electroanal. Chem.* **248**, 451 (1988).
3. S.-L. Yau, X. Gao, S.-C. Chang, B. C. Schardt, M. Weaver, *J. Am. Chem. Soc.* **113**, 6049 (1991).
4. B. M. Ocko, J. Wang, A. Davenport, H. Isaacs, *Phys. Rev. Lett.* **65**, 1466 (1990).
5. S. Manne, P. K. Hansma, J. Massie, V. B. Elings, A. A. Gewirth, *Science* **251**, 183 (1991).
6. J. V. Barth, H. Brune, G. Ertl, R. J. Behm, *Phys. Rev. B* **42**, 9307 (1990).
7. C. Woll, S. Chiang, R. J. Wilson, P. H. Lippel, *ibid.* **39**, 7988 (1989).
8. J. Perdereau, J. P. Biberian, G. E. Rhead, *J. Phys. F* **4**, 1978 (1974).
9. D. M. Zehner and J. F. Wendelken, in *Proceedings of the Seventh International Vacuum Congress and the Third International Conference on Solid Surfaces*, R. Dobrozemsky, Ed. (Berger and Sohne, Vienna, 1977), p. 517.
10. K. Yamazaki, K. Takayamagi, Y. Tanishiro, K. Yagi, *Surf. Sci.* **199**, 595 (1988).
11. U. Harten, A. M. Lahee, J. P. Toennies, C. Woll, *Phys. Rev. Lett.* **54**, 2619 (1985).
12. K. G. Huang, D. Gibbs, D. M. Zehner, A. R. Sandy, S. G. J. Mochrie, *ibid.* **65**, 3317 (1990).
13. A. R. Sandy, S. G. J. Mochrie, D. M. Zehner, K. G. Huang, D. Gibbs, *Phys. Rev. B* **43**, 4667 (1991).
14. A. Hamelin, *J. Electroanal. Chem.* **142**, 229 (1982).
15. J. P. Bellier and A. Hamelin, *C. R. Acad. Sci.* **280**, 1489 (1975).
16. M. S. Zei, G. Lehmpfuhl, D. M. Kolb, *Surf. Sci.* **221**, 23 (1989).
17. A. Friedrich *et al.*, *Chem. Phys. Lett.* **163**, 123 (1989).
18. G. Lupke *et al.*, *Phys. Rev. B* **41**, 6913 (1991).
19. N. J. Tao and S. M. Lindsay, *J. Appl. Phys.* **170**, 5143 (1991).
20. X. Gao, A. Hamelin, M. J. Weaver, *J. Chem. Phys.* **95**, 6993 (1991).
21. Single-crystal Au disk electrodes were aligned and polished within 0.1° of the <111> direction. Vacuum-sputtered and annealed electrodes were transferred through air to an electrochemical SXS cell constructed from Kel-F (*4*). After the cell has been filled with electrolyte, the cell is deflated, leaving a thin (~10 μm thick) capillary electrolyte film between the crystal face and a 6-μm-thick polypropylene x-ray window. Grazing-incident angle SXS measurements were carried out with focused, monochromatic (wavelength λ = 1.54 Å) synchrotron radiation at Brookhaven National Laboratory's National Synchrotron Light Source at beamline X22B. The longitudinal in-plane and transverse out-of-plane resolutions were 0.007 $Å^{-1}$ half width at half maximum (HWHM) and 0.06 $Å^{-1}$ HWHM, respectively (*22*). The (H,K,L) coordinate system is hexagonal (*13*) where $(H,K) = (H,K,0)$ lies within the surface plane and L is along the surface normal direction. For Au, the hexagonal lattice parameters are $a^* = b^* = 4\pi/\sqrt{3}a = 2.52$ $Å^{-1}$, $c^* = 2\pi/\sqrt{6}a = 0.89$ $Å^{-1}$, and $a = 2.885$ Å.
22. J. Wang, B. M. Ocko, A. J. Davenport, H. S. Isaacs, unpublished results.
23. A. Hamelin, personal communication.
24. ———, *J. Electroanal. Chem.* **144**, 365 (1983).
25. J. Lecoeur and A. Hamelin, *C. R. Acad. Sci. C* **279**, 1081 (1974).
26. C. L. Fu and K. M. Ho, *Phys. Rev. Lett.* **63**, 1617 (1989).
27. M. A. Van Hove *et al.*, *Surf. Sci.* **103**, 189 (1981); *ibid.*, p. 218.
28. V. Heine and L. D. Marks, *ibid.* **165**, 65 (1986).
29. D. M. Kolb and J. Schneider, *ibid.* **162**, 764 (1985).

30. This work was supported by the Division of Materials Research, U.S. Department of Energy, under contract DE-AC02-76CH00016.

4 October 1991; accepted 8 January 1992